Co^{2+} doped ZnS nanocrystals: structural, optical, magnetic and photoluminescence properties via co-precipitation method

E. Naga Jyothi[1,2], N.Ch. Anjaneyulu[2], Sk. Johny Basha[2], B.S.Anand Kumar[3], R.V.S.S.N. Ravikumar[2*]

[1]Department of Physics, Government Polytechnic College, Visakhapatnam-530007, A.P., India

[2]Department of Physics, Acharya Nagarjuna University, Nagarjuna Nagar-522510, Guntur, A.P., India.

[3]Department of Physics, Sree Dattha College of Engg & Science, Ibrahimpatnam-501510, Hyderabad, Telangana, India.

Abstract

Co^{2+} ions doped ZnS nanocrystals is produced by a straightforward co-precipitation technique. The produced nanocrystals' structural, optical, morphological, magnetic and photoluminescence properties were examined. Powder X-ray diffraction patterns reveal that prepared nanocrystals exhibit a cubic structure with an average crystallite size of 7 nm. Both SEM and TEM images depict stone-loke structures that are distributed non-uniformly. The presence of Co^{2+} ions within ZnS nanocrystals is confirmed through EDS analysis. The FT-IR spectrum displays characteristic absorption peaks corresponding to ZnS bonds, confirming Co ions incorporation into ZnS nanocrystals. The site symmetry of metal ions with their ligands can be determined additionally, crystal field (Dq) and inter-electronic repulsion (B and C) parameters computed using the optical absorption spectrum. The spin Hamiltonian parameters determined from EPR data are $g_{\parallel} = 2.66$ and $g_{\perp} = 2.86$. The octahedral site symmetry of Co^{2+} doped metal ions was established through optical and EPR measurements with host lattice. The PL spectrum exhibits emission bands in visible regions. CIE chromaticity coordinates are determined as (x, y) = (0.1774, 0.1236) which indicates that the blue region. The stability of Co^{2+} ion-doped ZnS nanocrystals is determined by TG-DTA assessment. According to the present investigation, Co^{2+} ions doped ZnS nanocrystals may be used in spintronics, LEDs and nanoscale quantum services.

Keywords: Nanocrystals, Cobalt ions, Spectroscopic studies, photoluminescence.

1. Introduction

Materials with hundreds or thousands of atoms make up nanocrystals and particles which have drawn a lot of interest recently. The development of science and technology is greatly

aided by semiconductors. Recent advances in nanotechnology will likely lead to the emergence of numerous novel intelligent materials and advanced gadgets[1]. Semiconductor nanocrystals are excellent detectors that are of great interest to the systematic and technical communities due to their remarkable magnetic, optical and luminescent characteristics[2]. Among the several II-IV semiconductor compounds, ZnS is a significant and eco-friendly chemical that has a broad straight bandgap making it a suitable host for transition metal ions. Their adaptability makes them attractive parts for a wide range of applications such as medication delivery systems, biological sensors, solar devices, photodetectors, light-emitting diodes (LEDs), lasers, photocatalysis, display devices and other optoelectronic devices[3-4]. In the semiconductor family, Zinc sulfides (ZnS, PbS, SnS and CdS) and selenides (ZnSe, PbSe, SnSe and PbSe) have emerged as particularly interesting materials in recent years[5]. ZnS nanoparticles are a common nontoxic wide band gap semiconductor material with good light emitters in the blue and ultraviolet wavelength ranges. These materials are used in many different applications, including phosphors, solar cells and infrared windows[6]. Compared to existing II-VI semiconductor nanoparticles, ZnS has great promise for electrochemical nanotechnology including anti-reflection coatings, nanosensors, nanogenerators and nanodevices[7]. One of the greatest n-type semiconductors is ZnS, which exists in two crystalline forms with slightly varying bandgap energies.

Transition metal ions provide novel ways to modify the optical, electrical, magnetic and physical properties of inorganic semiconductor nanocrystals[8]. However, selecting an appropriate dopant is crucial for enhancing the suitability of the host system. Using different metal dopants, such as Mg, Co, Mn, Ni and Cd has shown encouraging results in previous decades[9]. Among them, Co^{2+} ions as dopants improve their visible light absorption and high magnetic moment due to their 3d transition and potential properties. Reasons for selecting Co^{2+} as a dopant are (i) Co^{2+} is a good magnetic material (ii) Co^{2+} with an ionic radius of 0.72 Å closely matches the size of the zinc ion (0.74 Å) and hence Co^{2+} can easily substituted at that Zn location while preserving ZnS crystalline structure[10]. It also demonstrated interesting optical properties. Consequently, Co-doped ZnS offers an excellent chance to study its magnetic and photoluminescent characteristics.

Several effective methods exist for synthesizing ZnS nanocrystals, including Mechanical alloying[11], Solvothermal method[12], Facile synthesis Hydrothermal method[13] and Co-precipitation method[14]. The prospective uses of these methods in scientific and commercial research led to their selection. Of these methods, the co-precipitation method stands out for its convenience in achieving mass production at a moderate cost its eco-friendliness, low-

temperature requirement, minimal energy consumption and producing small particles. In the present study, we report crystal structure, distortion in the lattice, energy level structure, site symmetry, bonding nature and luminescent properties. Several spectroscopic techniques are applied to the synthesized material to obtain a comprehensive perspective.

2. Experimental details

2.1 Materials

Analytical grade, sodium sulfide (Na_2S), zinc acetate ($Zn(CH_3COO)_2$. $2H_2O$) and transition metal of cobalt nitrate ($Co(NO_3)_2$) are procured from Merck Chemicals, Mumbai, India. All of the chemical reagents used in this experiment are analytical grade and without further purification.

2.2 Preparation of Co^{2+} doped ZnS nanocrystals

Initially, 0.5% zinc acetate dissolved in a mixture of deionized water and ethanol. The mixture was magnetically stirred until a homogenous white solution was obtained at 80 ℃. After 10 minutes, sodium sulfide (0.5 mol%) solution was added to the previous solution in an equal volume mixture of deionized water and ethanol while stirring continuously. Cobalt nitrate ($Co(NO_3)_2$), a concentration of 0.01 mol% was added to solution with continuous stirring for 2 h. Precipitation was produced once the reaction was completed. The solution is centrifuged at 10,000 rpm for 30 minutes and dried in air at 120 ℃ for 2h.

2.2 Characterization

Powder X-ray diffraction was performed with a SHIMADZU LABX XRD-6100 diffractometer CuKα radiation (1.5406 Å) within the range of 10º-70 º. A prepared sample's surface morphology and chemical analysis are characterized using a ZEISS VO18 microscopy SEM with EDS attachment. TEM images were obtained using the HITACHI H-7600 transmission electron microscope (TEM) and CCD CAMERA system AMTV-600 with samples dispersed in ethanol. Optical absorption was recorded by UV-VIS-NIR JASCO V-670 spectrophotometer in the range of 200-1400 nm. EPR spectrum was captured using a JES-FA 200 electron spin resonance spectrometer that was field-modulated at 100 KHz and operated at X-band frequencies. The photoluminescence spectrum was captured using a Horiba Fluromax-4 spectrophotometer with excitation provided by both continuous (450 W) and pulsed (35 W) Xenon lamps. SHIMADZU DTG-60H was used to perform differential thermal analysis (DTA) and thermal gravimetric (TG) analysis on the powder sample.

Figure captions

Fig 1: XRD patterns of Co^{2+} doped ZnS nanocrystals

Fig 2**:** SEM images of Co^{2+} doped ZnS nanocrystals

Fig 3**:** EDS spectrum of Co^{2+} doped ZnS nanocrystals

Fig 4: SEM histogram of Co^{2+} doped ZnS nanocrystals

Fig 5: TEM images of Co^{2+} doped ZnS nanocrystals

Fig 6**:** TEM histogram of Co^{2+} doped ZnS nanocrystals

Fig 7**:** FTIR spectrum of Co^{2+} doped ZnS nanocrystals

Fig 8**:** Optical absorption spectrum of Co^{2+} doped ZnS nanocrystals

Fig 9: Tauc plot of the optical band gap energy of CO^{2+} doped ZnS nanocrystals

Fig 10: EPR spectrum of Co2+ doped ZnS nanocrystals

Fig 11: PL emission of Co^{2+} doped ZnS nanocrystals

Fig 12: CIE diagram of Co^{2+} doped ZnS nanocrystals

Fig 13**:** TGA and DTA cures of Co^{2+} doped ZnS nanocrystals

3. Results and discussions

3.1 Structural analysis

Figure 1 shows X-ray diffraction pattern of Co^{2+} doped ZnS nanocrystals. Three distinct diffraction peaks are detected at 2θ values of 28.67, 48.07 and 56.57 corresponding to lattice planes (1 1 1), (2 2 0) and (3 1 1) respectively. The phase structure of prepared sample is cubic and planes matched with standard JCPDS file No. 05-0566. XRD studies reveal the intensity of (1 1 1) plane is greater than (2 2 0) and (3 1 1) planes which indicates that grain growth orientation aligns predominantly along (1 1 1) plane.

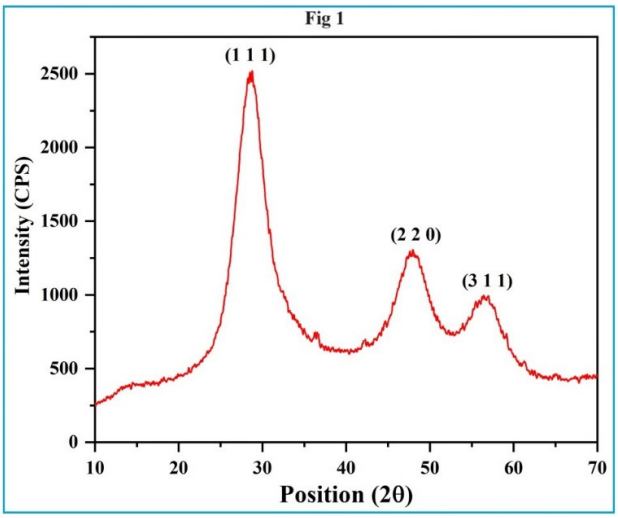

XRD patterns generally shift towards higher angles with a concurrent decrease in lattice cell parameters. This phenomenon occurs because the ionic radius of the host exceeds that of

the dopant resulting in tensile strain[15]. The computed lattice cell parameters in this work, a = 0.5347 nm is less than the usual value (a = 0.5406 nm) for cubic ZnS nanocrystals. The ionic radius of Zn^{2+} (0.074 nm) is larger than that of Co^{2+} (0.072) this results reduction in lattice cell parameters induces tensile strain and shifts the XRD pattern in the direction of greater Bragangle[16]. Debye Scherrer's formula is used to get the average crystallite size, which is as follows:

$$D = \frac{K\lambda}{\beta cos\theta} \quad (1)$$

Where β is full-width at half-maximum, K is a geometric factor (K = 0.9), θ is Bragg angle and λ is the wavelength of incident CuKα radiation. The average crystallite size was calculated as 7 nm. Microstrain (ε) and dislocation density (δ) values were evaluated as 10.64×10^{-3} and 9.76×10^{16} lines/m^2 using the following relations as

$$\varepsilon = \frac{\beta cos\theta}{4} \quad (2)$$

$$\delta = \frac{1}{D^2} \quad (3)$$

3.2 Morphological studies

The SEM technique provides information on surface morphology and particle distribution and is a valuable tool for topographic analysis of prepared material. Figure 2 depicts SEM images of Co^{2+} doped ZnS nanocrystals captured in different magnifications of 1.5 µm and 3 µm consisting of stone-like structures. The grain size was evaluated using SEM images by counting 50 particles at a magnification of 3 µm to reduce error and creating a histogram plot as shown in Figure 3 evaluated grain size was 28 nm. The EDS pattern reveals the presence of Zn, S and Co elements as shown in Figure 4 and the absence of any additional peaks associated with contaminants or impurities attests to the synthesized sample purity. The compositions of the acquired elements Zn, S and Co which are specified in the table in the inset of Figure 4 align well with the experimental stoichiometric calculations.

Fig 2

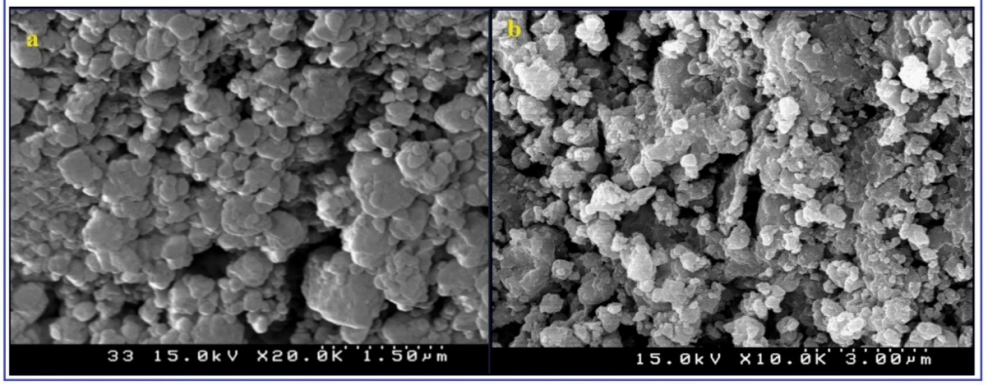

Fig 3

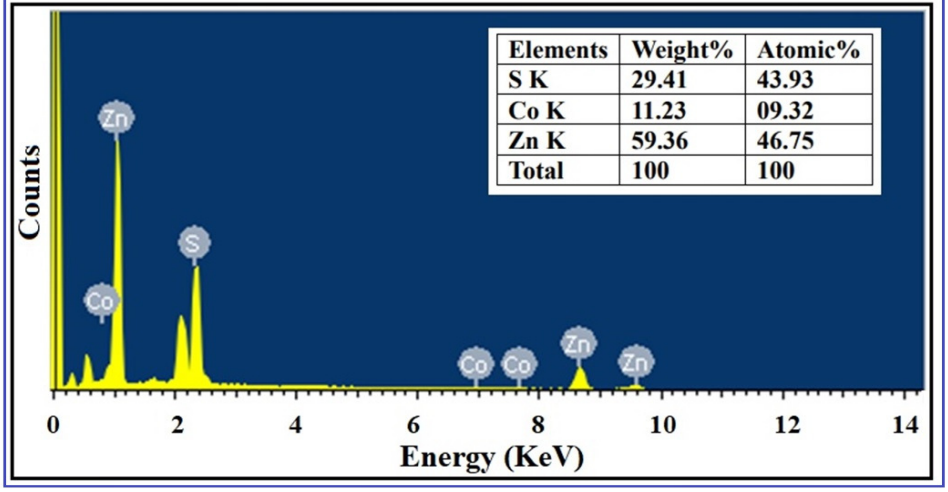

Fig 4

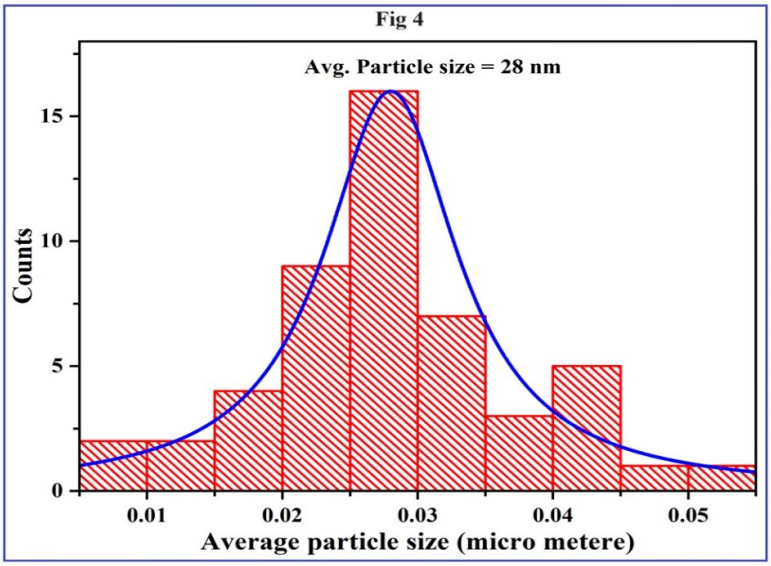

The microstructures of the prepared sample was further analyzed using TEM. Figure 5 depicts TEM images measured at different magnifications of 100 and 500 nm. The prepared sample possesses a stone-like structure morphology with some agglomeration. ImageJ software and Gaussian fitting of the size distribution were used to determine the average particle size value. The distribution cure yielded an average particle size of 19 nm as illustrated in Figure 6. The estimate of particle size value derived from TEM images good agreement with the XRD data result.

Fig 5

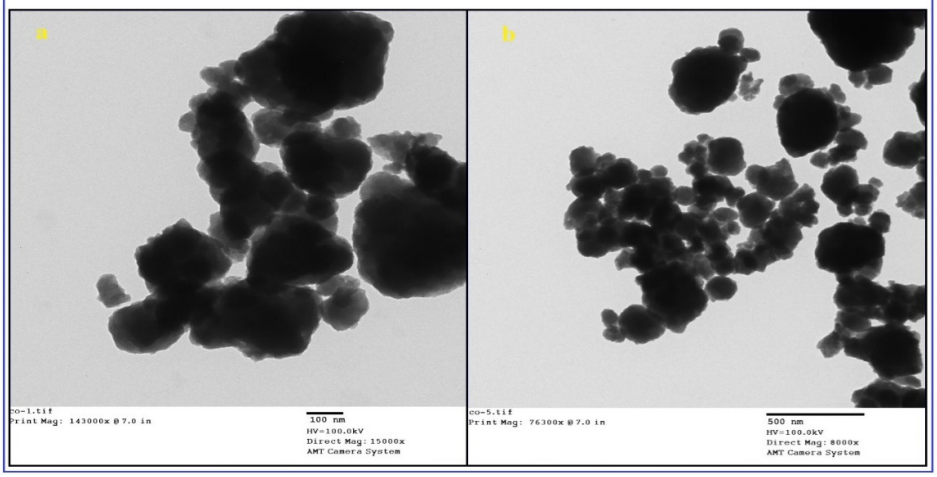

Fig 6

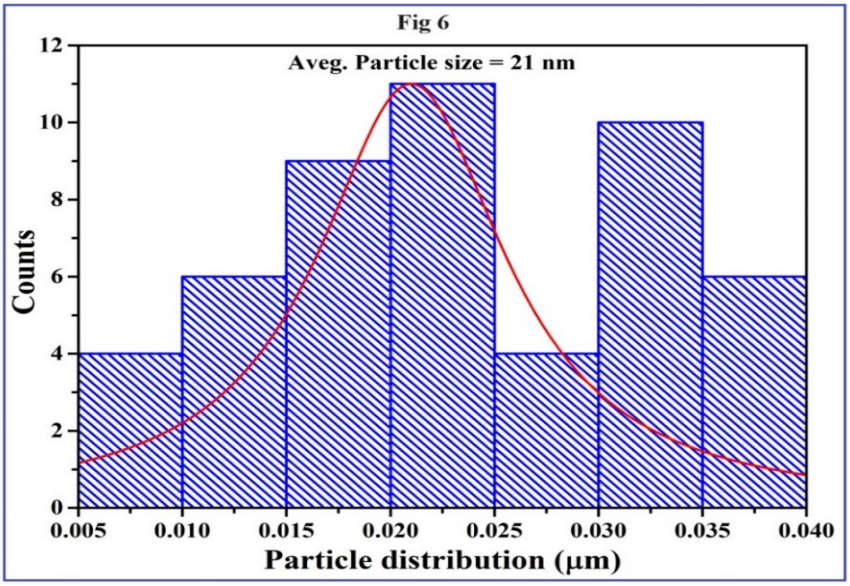

3.3 FT-IR analysis

The existence of several functional groups and adsorbing chemical species in the synthesis of Co^{2+} doped ZnS nanocrystals can be identified through the FT-IR spectrum as illustrated in Figure 7. It exhibits numerous absorption peaks and bands due to the multiple vibration modes associated with its constituent groups. The peaks at 3731 and 3400 cm^{-1} correspond to the stretching of O-H bonds absorbed on the surface of the H_2O molecule[17]. The band detected at 2306 cm^{-1} is attributed to the stretching of C-H bonds[18]. The absorption bands at 1563 and 1408 cm^{-1} are associated with the C=O stretching mode for a carboxylic group (-COOH) of zinc acetate[19]. The band at 1340 cm^{-1} is assigned to -OH bending vibration[20]. The C-C mode stretching frequency was observed at 1019 and 936 cm^{-1} representing the presence of ZnS nanocrystal interaction[19]. The vibrational peaks at 673 and 477 cm^{-1} are attributed to

Zn-S bonds[21]. Position and their assignment of Co^{2+} doped ZnS nanocrystals as shown in Table 1.

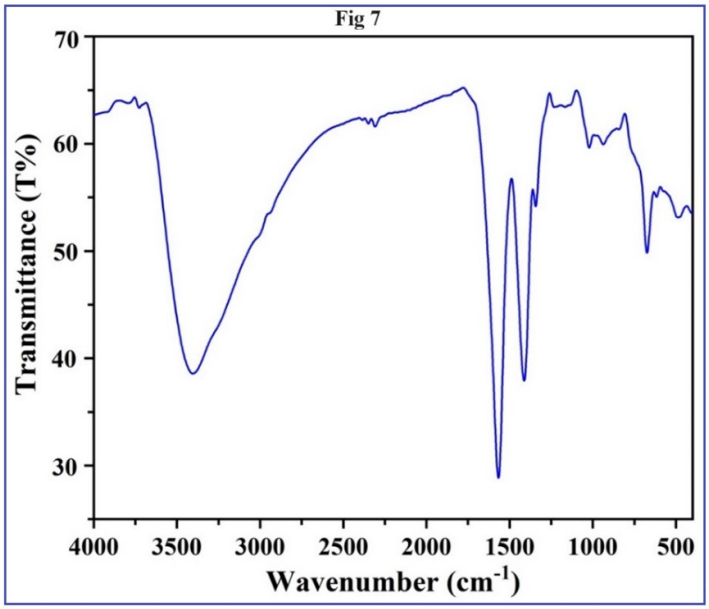

Table 1 Position and their assignment of Co^{2+} doped ZnS nanocrystals from FT-IR analysis

Band positions (cm^{-1})	Band assignment
3730, 3402	O-H stretching
2306	C-H stretching
1561, 1418	C=O stretching
1340	-OH bending
936,1019	C-C stretching
477, 673	Zn-S stretching

3.4 Optica absorption studies

The d^7 configuration of Co^{2+} in a weak octahedral crystal field produces multiple quartet states $^4T_{1g}(F)$, $^4T_{2g}(F)$, $^4A_{2g}(F)$ and $^4T_{1g}(P)$ in addition to doublet states $^2A_{1g}(G)$, $^2T_{1g}(G)$, $^2T_{2g}(G)$ and $^2E_g(G)$. Among these $^4T_{1g}(F)$ is the ground state. $^2E_g(G)$ would represent the ground state only in strong crystal fields (Dq = 1500 cm^{-1}). In the current scenario, similar to the intermediate crystal fields $^4T_{1g}(F)$ remains the ground state as evidenced by present case with Dq = 970 cm^{-1}. Consequently, it is reasonable to assume three spin-allowed transitions: $^4T_{1g}(F) \rightarrow {}^4T_{2g}(P)$, $^4T_{1g}(F) \rightarrow {}^4A_{2g}(F)$ and $^4T_{1g}(F) \rightarrow {}^4T_{2g}(F)$. Among these transitions, $^4T_{1g}(F) \rightarrow {}^4A_{2g}(F)$ is anticipated to be weak due to involving a double electron jump ($t^5_{2g}e^2_g \rightarrow t^3_{2g}e^4_g$)[22].

Figure 8 displays the optical absorption spectrum of Co^{2+} ions doped ZnS nanocrystals. Absorption spectrum exhibits five bands at 477, 494, 505, 627 and 1157 nm (20959, 20237, 19796, 15944 and 8641 cm^{-1}) respectively. Two bands at 1157 and 477 nm correspond to two

spin-allowed transitions from ground state $^4T_{1g}(F)$ to excited states $^4T_{2g}(F)$ and $^4T_{1g}(P)$ respectively. Consequently, the three bands are associated with transitions $^4T_{1g}(F) \rightarrow {}^2A_{2g}(G)$, $^2T_{1g}(G)$ and $^2T_{2g}(G)$ in that order. The energy ratios of transitions $^4T_{1g}(F) \rightarrow {}^4A_{2g}(F)$: ν_2 and $^4T_{1g}(F) \rightarrow {}^4T_{2g}(F)$: ν_1 are almost constant between 1.9 1nd 2.2 in O_h symmetry theoretical framework[23]. From the energy matrix of the d^7 configuration, crystal field (Dq) and inter-electronic repulsion (B and C) parameters are calculated. The measured band locations at Dq = 970, B = 870 and C = 3850 cm^{-1} are well-fitted by these parameters. The free ion value of B is 1120 cm^{-1} for Cobalt ion[24]. A 22% decrease in B's free ion is indicative of a significant covalent bond. The features may result from distortion caused by the octahedral symmetry of Co^{2+} site in the material. Table 2 provides optical head data along with their assignments.

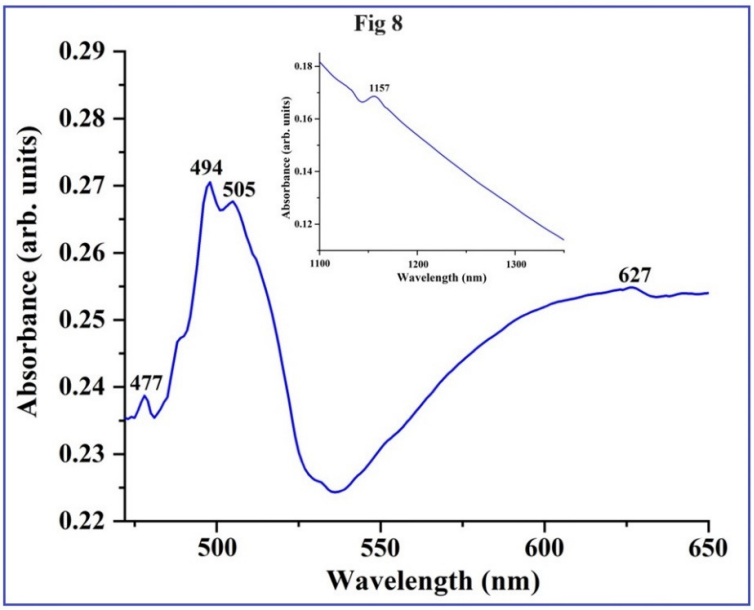

Table 2 Optical absorption band head data of Co^{2+} ions doped ZnS nanocrystals

Transitions from $^4T_{1g}(F)$	Observed band positions		Calculated
	Wavelength (nm)	Wavenumber (cm^{-1})	Wavenumber (cm^{-1})
$^4T_{1g}(P)$	477	20959	20542
$^4A_{2g}(F)$	494	20237	19721
$^2T_{1g}(G)$	505	19796	20106
$^2T_{2g}(G)$	627	15944	16164
$^4T_{2g}(F)$	1157	8641	8521

Tauc's plot provides a clearer method for determining the optical energy bandgap in semiconductors. The energy bandgap (Eg) can be ascertained through simple optical absorption allowing for electron excitation from the valence band to the conduction band. Tauc put

forward a correlation between the nanoparticle's absorption coefficient (α) and energy of the incident photons[25] as

$$\alpha h\nu = A\left(h\nu - E_g\right)^{\frac{n}{2}} \quad (4)$$

Here A represents a constant and the exponent n varies according to a type of transition with n = ½ for direct transitions. The bandgap energy was approximated by graphing $(\alpha h\upsilon)^2$ vs hυ as illustrated in Figure 9. The energy bandgap value is 1.75 eV obtained by extrapolating the straight line to the X-axis.

Fig 9

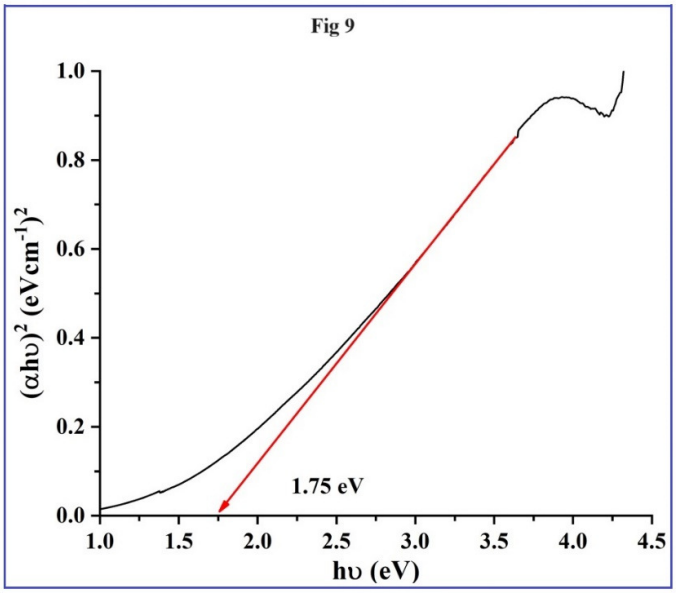

EPR studies

The Co^{2+} ions exhibit distinct characteristics when present in tetrahedral and octahedral coordination showing variations in their spin states between low and high spins. A ground state Kramer's doublet with g = 4.33 is produced by splitting the lowest orbital triplet state in a $3d^7$ structure which exhibits precise octahedral symmetry[26]. For the octahedral, the real g factor varies from 2 to 9 in terms of spin-orbit coupling and excited orbital interactions. The high-spin Co^{2+} energy's deformed tetrahedral shape is either smaller in the ±3/2 state or ±1/2 state[27]. As a result, the g values become sensitive to changes in the crystal field and become anisotropic. EPR spectrum of Co^{2+} doped ZnS nanocrystals exhibit resonance lines at $g_{\parallel} = 2.66$, $g_{\perp} = 2.86$ as illustrated in Figure 10. Octahedral symmetry is responsible for $g_{\parallel} = 2.66$ line whereas a random distribution of distortion is cause of $g_{\perp} = 2.86$ line. The g value of the prepared sample exhibiting $g_{\parallel} < g_{\perp}$indicating the presence of a dynamic Jahn-Teller effect, where the axial ligands are slightly different compared to a previous report[28]. The effective g value is

$$g_{eff} = \frac{g_{\parallel}+2g_{\perp}}{3} = 2.79 \quad (5)$$

The parameters of covalency (κ_0) have been assessed using the relation by correlating the optical and EPR spectra[29].

$$g = \frac{10}{3} + \kappa_0 - \frac{15}{2}\left(\frac{\lambda}{\Delta}\right) \quad (6)$$

Where Δ is the energy of transition $^4T_{1g}(F) \rightarrow {}^4T_{2g}(F)$, g is the measured g-factor and λ means spin-orbit coupling constant (-178 cm^{-1} for Co^{2+}). The value of κ_0 lies between 1 and 0.5, the limits of pure ionic and covalent nature respectively. Based on the current study, the computed value of κ_0 is 0.694 suggesting that bonding between the ligands and Co^{2+} is predominantly ionic.

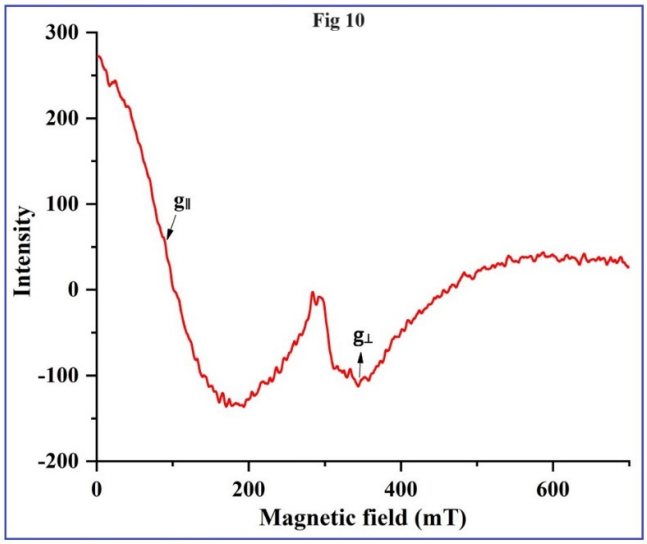

PL analysis

The PL spectrum of Co^{2+} doped ZnS nanocrystals obtained at an excitation wavelength of 325 nm is depicted in Figure 11. The PL spectrum exhibits three emission peaks at 419, 525 and 609 nm corresponding to violet, green and orange regions. The recombination between valence and donor linked to sulfur vacancies is responsible for a peak at 419 nm[30]. Another peak at 525 nm in the green region is attributed to defective states caused by the presence of doped Co^{2+} ions[31]. Luminescent centers comprising cobalt ions are established through the incorporation of cobalt into the ZnS host lattice. Co^{2+} acts as a sensitizing agent, its presence in the host lattice will accelerate the radiative recombination processes[32]. Additional peak at 609 nm is attributed to recombination of electron hole pairs associated with surface states and sulfur vacancy centers[31].

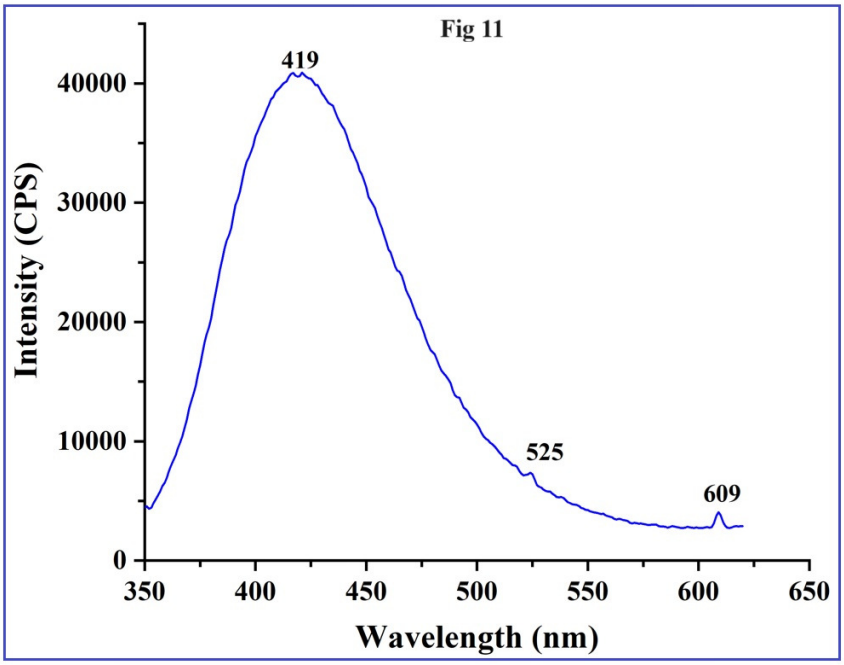

The CIE color chromaticity coordinates help precisely ascertain the prepared sample emission color vision. Figure 12 displays CIE chromaticity coordinates of Co^{2+} doped ZnS nanocrystals extracted from emission spectrum. The CIE parameters calculated using MATLAB software indicate coordinates in a blue region with values of (x, y) = (0.1774, 0.1236). The quality of color light source (CCT) is determined using the McCamy formula[33]. The evaluated CCT and CIE values are 4009 K and 75 % respectively. From the CIE and CCT values, the present sample may be useful for blue LED display devices.

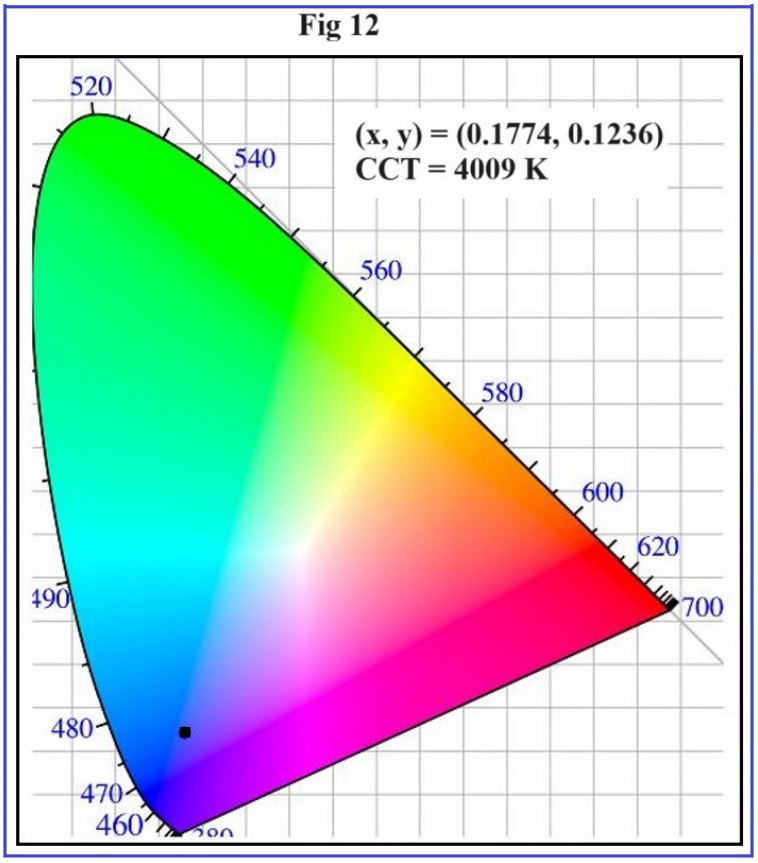

TG/DTA analysis

Mutual TGA and DTA analysis plots of Co^{2+} ions doped ZnS nanocrystals as shown in Figure 13. TG-DTA thermogram is recorded from ambient temperature to 1100 ℃ in a nitrogen environment increased by 10 ℃ min^{-1}. Four distinct endothermic peaks exist on DTA cure in succession up to 1100 ℃. Based on TG analysis, the first endothermic peak on the DTA at around 57 ℃ which corresponds to 4.9% weight loss signifies the physical adsorbed water being stripped off. The second endothermic peak at 342 ℃ with a corresponding measured weight loss of 8% demonstrates the release of Co^{2+} ions from ZnS matrix. The third endothermic peak at 671 ℃ gives melting of the substance with a weight loss of 1.7%. A final endothermic peak at 969 ℃ is caused by sulfur breaking down with a corresponding weight loss of 5.2%. The total weight loss from room temperature to 1100 ℃ is 33.8%.

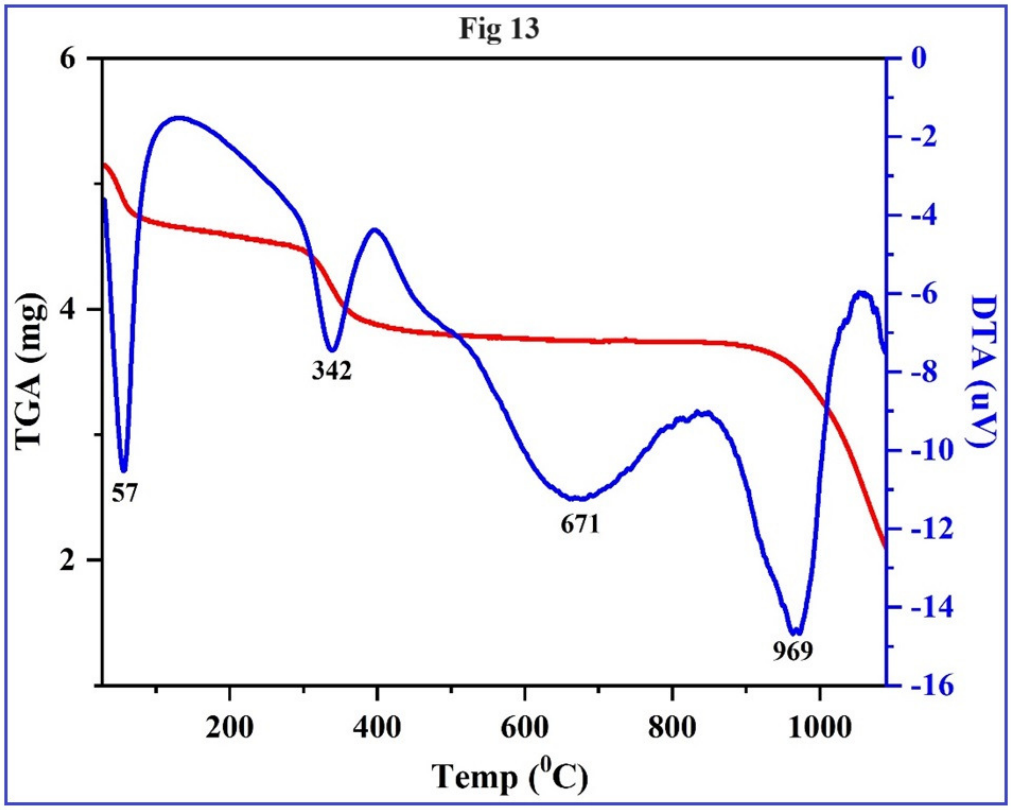

Conclusions

Co^{2+} ions doped ZnS nanocrystals was successfully produced via the co-precipitation technique. X-ray diffraction pattern revealed the structure was cubic. The average crystallite size was evaluated using Scherer's method to be 7 nm within the nanoscale range. Both SEM and TEM images depict stone-like structures that are non-uniformly distributed. Zn, S and Co components were verified to be present in the produced sample by the EDS spectrum. The basic vibration bands of host molecules and doped metal ions were verified by the FTIR spectrum. The determined crystal field (Dq) and inter-electronic repulsion (B, C) parameters were calculated from optical absorption data to be Dq = 980 cm^{-1} and B = 890 cm^{-1}, C = 3850 cm^{-1} respectively. Comparing optical and EPR spectra verified that connection between Co^{2+} and its ligands is partly ionic and that ions have a distorted site symmetry. The PL spectrum exhibits three peaks at 419, 525 and 609 nm corresponding to blue, green and orange emissions respectively. The evaluated CCT and CRI values of 4009 K and 75% respectively, suggest that the material could be suitable for blue LEDs and solid-state lighting devices. TG-DTA curves illustrate the produced sample thermal degradation at various temperatures with a total weight loss of 33.87%. The results suggest that the prepared material is useful for spintronic applications.

Acknowledgments

The Authors thanks to the MHRD project, New Delhi providing financial assistance to the Department of Physics, ANU to carry out the present research work. Authors thank the Director, Centralized Laboratory, ANU and Department of Physics, University of Kerala for providing Ultra-centrifuge and Photoluminescence facilities. Authors also thank The Head, SAIF, IIT Madras for providing EPR facility.

Authors contributions

E. Naga Jyothi: Writing-original draft, conceptualization and methodology. **N.Ch. Anjaneyulu:** Editing, writing review, investigation and methodology. **Sk. Johny Basha:** Methodology and editing. **B.S. Anand Kumar:** Editing, Writing review. **R.V.S.S.N. Ravikumar:** Conception, supervision, review and editing.

Data availability

The authors confirm that the information/data of the present research article are available inside the article.

Declarations Conflict of interest The authors declare that they have no known competing financial interests or personal relationships that could appear to have influenced the work reported in this paper.

References

1. Sk. Johny Basha, V. Khidhirbrahmendra, J. Madhavi, U. Udayachandran Thampy, Ch. Venkata Reddy, R. V. S. S. N. Ravikumar, Structural, optical, magnetic and thermal investigations on Cr^{3+} ions doped ZnS nanocrystals by co-precipitation method, J Sci Adv Mater Devices, **4,** 260-266 (2019). https://doi.org/10.1016/j.jsamd.2019.03.002
2. B. Huang, R. Xu, L. Zhang, Y. Yuan, C.h. Lu, Y. Cui, J. Zhang, Effect of Cu/In ratio and shell thickness on the photo-stability of $CuInS_2$/ZnS nanocrystals, J Mater Chem C, **5,** 12151-12156 (2017). https://doi.org/10.1039/C7TC04032F
3. B. Poornaprakash, K. Naveen Kumar, U. Chalapathi, M. Reddeppa, P.T. Poojitha, S.H. Park, Chromium doped ZnS nanoparticles: chemical, structural, luminescence and magnetic studies, J Mater Sci Mater Electron, **27(6),** 6474–6479 (2016). DOI: 10.1007/s10854-016-4588-0
4. A. Dhupar, S. Kumar, H.S. Tuli, A.K. Sharma, V. Sharma, J.K. Sharma, In-doped ZnS nanoparticles: structural, morphological, optical and antibacterial properties, Appl Phys A, **127,** 263 (2021). https://doi.org/10.1007/s00339-021-04425-9

5. B. Lalithadevi, K. Mohan Rao, D. Ramananda, Investigations on structural and optical properties of starch capped ZnS nanoparticles synthesized by microwave irradiation method, Chem Phys Lett, **700,** 74-79 (2018). https://doi.org/ 10.1016/j.cplett.2018.04.010
6. W. Li, Q. Y. He, Y. Z. Wang, T. Wang, Investigations of press-induced band gap changes in PbS, Chem Phys Lett, **687,** 101-105 (2017). https://doi.org/10. 1016/j.cplett.2017.09.002
7. K. Vijai Anand, Improved structural, optical and photoluminescence properties of EDTA capped Zinc Sulfide Nanoparticles for optoelectronic applications, J Clust Sci, **32,** 155-161 (2021). https://doi.org/10.1007/s10876-020-01772-0
8. Z.J. Li, E. Hofman, A. Blaker, A.H. Davis, B. Dzikovski, D.K. Ma, W. Zheng, Interface engineering of Mn-doped ZnSe-based core/shell nanowires for tunable host-dopant coupling, ACS Nano, 11(12), (2017) 12591-12600. https:// doi.org/10.1021/acsnano.7b06773.
9. S. Upputuri, S. Lakshmanan, N. Ramalakshmi, S.A. Antony, Investigating on Structural, Optical, Magnetic and Photocatalytic Activities of ZnS and Co^{2+}: ZnS NPs Synthesized by Hydrothermal Process Under MeB Dye, Res Sq, 1-12 (2021). https://doi.org/10.21203/rs.3.rs-866114/v1
10. E. Elsi, S. Mohanapriya, K. Pushpanathan, Observation of novel superparamagnetism in ZnS:Co Quantum Dots, J Supercond Nov Magn, **33,** 3223-3240 (2020). https://doi.org/10.10007/s10948-020-05573-4
11. A. Dhara, S. Sain, S. Das, S.K. Pradhan, Microstructure, optical and electrical characterizations of Mn-doped ZnS nanocrystals synthesized by mechanical alloying, Mater Res Bull, **97,** 169-175 (2018). http://dx.doi.org/10.1016/j.materresbull.2017.08.060
12. K. Ashwini, Yashaswini, C. Pandurangappa, Solvothermal synthesis, characterization and photoluminescence studies of ZnS: Eu nanocrystals, Opt Mater, **37,** 537-542 (2014). https://doi.org.10.1016/j.optmat.2014.07.019
13. W. Zhao, Z. Wei, L. Zhang, X. Wu, X. Wang, J. Jiang, Optical and magnetic properties of Co and Ni co-doped ZnS nanorods prepared by hydrothermal method, J Alloys Compd, **698,** 754-760 (2017). https://doi.org/10.1016/j.jallcom.2016.12.127
14. M. Stefan, I.D. Vlaicu, L.C. Nistor, D. Ghica, S.V. Nistor, Origin and chemical composition of the amorphous material from the intergrain pores of self-assembled cubic ZnS: Mn nanocrystals, Appl Surf Sci, **426,** 342-350 (2017). https://doi.org/10.1016/j.apsusc.2017.07.172

15. B. Babu, G.T. Rao, V.P. Manjari, K. Ravindranadh, R.J. Stella, R.V.S.S.N. Ravikumar, Sonochemical assisted synthesis and spectroscopic characterization of Fe^{3+} doped ZnO diluted magnetic semiconductor, J Mater Sci Mater Electron, **25,** 4179-4186 (2014). DOI: 10.1007/s10854-014-2146-1
16. Sk. Johny Basha, V. Khidhirbrahmendra, M. Avinash, U. Udayachandran Thampy, Ch. Venkata Reddy, R.V.S.S.N. Ravikumar, Structural, spectral, magnetic and thermal properties of VO^{2+} doped ZnS nanocrystals by co-precipitation method, J Mater Sci Mater Electron, **29,** 6105-6112 (2018). https://doi.org/10.1007/s10854-018-8586-2
17. S. Vijayan, D. Chandra Sekhar, G. Umadevi, M. Sundararajan, R. Mariappan, Investigation of Structural, Optical and Antibacterial Activity of ZnS Nanoparticles, J Clust Sci, **32,** 1601–1608 (2021). https://doi.org/10.1007/s10876-020-01923-3
18. S. Mandal, Sk. Irsad Ali, A. Chandra Mandal, Investigation of structural, optical and photoluminescence properties of the sol-gel synthesized powder ZnS nanoparticles, Appl Phys A, **129,** 219 (2023). https://doi.org/10.1007/s00339-023-06499-z
19. A. Dhupar, S. Kumar, H.S. Tuli, A.K. Sharma, V. Sharma, J.K. Sharma, In-doped ZnS nanoparticles: structural, morphological, optical and antibacterial properties, Appl Phys A, **127,** 263 (2021). https://doi,org/10.1007/s00339-021-04425-9
20. L.Y. Wang, M.J. Wang, Removal of heavy metal ions by poly (vinyl alcohol) and carboxymethyl cellulose composite hydrogels prepared by a freeze-thaw method. ACS Sustain Chem Eng, **4,** 2830-2837 (2016). https://doi.org/10.1021/acssuschemeng.6b00336
21. S.C. Tudu, J. Kusz, M. Zubko, A. Bhattacharjee, Structural, morphological and optical characterization of green synthesized ZnS nanoparticles using Azadirachta Indica (Neem) leaf extract, Int J Nano Dimens, **11(2),** 99-111 (2020). https://hdl.handle.net/20.500.12128/17713
22. C. V. Reddy, L. V. Krishna Rao, D. V. Satish, J. Shim, R. V. S. S. N. Ravikumar, Structural and spectral characterization of Co^{2+}- and Ni^{2+}-doped CdO powder prepared from solution at room temperature, J Appl Spectrosc, **82(5),** 760-766 (2015). DOI 10.1007/s10812-015-0177-x
23. JaesoolShim, Ch. VenkataReddy, G.V.S.S. Sarma, P. Narayana Murthy, R.V.S.S.N.Ravikumar, Effect of Co^{2+} and Ni^{2+}- doped zinc borate nano crystalline powders by co-precipitation method, Spectrochim Acta A Mol Biomol Spectros, **142,** 279–285 (2015). http://dx.doi.org/10.1016/j.saa.2015.02.008
24. B.N. Figgis, Introduction to Ligand Fields, Wiley Eastern, New Delhi, 1976.

25. S. Elsi, S. Mohanapriya, K. Pushpanathan, Observation of novel superparamagnetism in ZnS: Co Quantum Dots, J Supercond Nov Magn, **33,** 3223-3240 (2020). https://doi.org/10.1007/s10948-020-05573-4
26. S. Kumar, J.K. Sharma, Stable phase CdS nanoparticles for optoelectronics: a study on surface morphology, structural and optical characterization, Mater Sci-Pol, **34(2),** 368–373 (2016). https://doi.org/10.1515/msp-2016-0033
27. M. Surya Sekhar Reddy, C. Sai Vandana, Y.B. Kishore Kumar, Tailoring the Inherent Magnetism of N: CdS Nanoparticles with Co^{2+} doping, Indian J Sci Technol, **16(27),** 2024-2034 (2023). https ://doi.org/10.17485/IJST/v16i27.596
28. R.V.S.SN. Ravikumar, A.V. Chandrasekhar, B.J. Reddy, Y.P. Reddy, J. Yamauchi, Spectroscopic investigations on Co(II) doped ZAPH and CAPH crystals, Ferroelectrics, **274,** 127-134 (2002). https://doi.org/10.1080/00150190213966
29. W. Low, Paramagnetic and optical of divalent cobalt in cubic crystalline fields, Phys Rev, **109,** 256 (1957). https://doi.org/10.1103/PhysRev.109.256
30. P.K. Singh, M. Kumar, A. Kumar, S. Singh, S. Sundaram, A.C. Pandey, Photoluminescence investigations of transition metal (Ni, Co) doped ZnS nanocrystals, J Adv Sci Res, **12,** 320-328 (2021). https://doi.org/10.55218/JASR.s2202112338
31. M.S. Akhtar, Y.G. Alghamdi, M.A. Malik, R.M. Khalil, S. Riaz, S. Naseem, Structural, optical, magnetic and half-metallic studies of cobalt doped ZnS thin films deposited via chemical bath deposition, J Mater Chem C, **3(26),** 6755-6763 (2015). DOI: 10.1039/c5tc00557d
32. R. Sarkar, C.S. Tiwary, P. Kumbhakar, A.K. Mitra, Enhanced visible light emission from CO^{2+} doped ZnS nanoparticles, Phys B Condens Mater, **404,** 3855-3858 (2009). https://doi.org/10.1016/j.physb.2009.07.106
33. C.S. McCamy, Correlated color temperature as an explicit function of chromaticity coordinates, Color Res Appl, **17,** 142-144 (1992). https://doi.org/10.1002/col.5080170211